Green
Chemistry

Accepted Manuscript

Nanoclusters of Cu (II) Supported on Nanocrystalline W (VI) Oxide: A Potential Catalyst for Single-Step Conversion of Cyclohexane to Adipic Acid

Shankha S. Acharyya,[a] Shilpi Ghosh,[a] and Rajaram Bal[a,]*

[a]Catalytic Conversion & Processes Division, CSIR-Indian Institute of Petroleum, Dehradun 248005, India

Corresponding author. Tel.: +91 135 2525917; Fax: +91 135 2660202

E-mail addresses: raja@iip.res.in

Keywords: Cu (II) nanoclusters • nanocrystalline W (VI) oxide • cyclohexane • adipic acid • selective oxidation

Abstract: A facile hydrothermal synthesis method is developed to prepare Cu (II) nanoclusters supported on nanocrystalline W (VI) oxide catalyst with size between 35-65 nm. Detailed characterization of the material was carried out by XRD, XPS, SEM, TEM, STEM-Mapping, Raman, FTIR, TGA, and ICP-AES. The catalyst was highly active for selective oxidation of cyclohexane to adipic acid with H_2O_2. The influence of reaction parameters such as temperature, substrate to oxidant molar ratio, reaction time, etc. were investigated in detail. The reusability of the catalyst was tested by conducting same experiments with the spent catalyst and it was found that the catalyst did not show any significant activity loss even after 4 reuses. A cyclohexane conversion of 75% with 88% adipic acid selectivity was achieved over this catalyst at 70 ºC temperature.

1. Introduction

Adipic acid (AA) is one of the most important commodity chemicals worldwide.[1] With a projected global market size of more than 6 billion pounds by 2017, AA serve as a versatile building block for an array of processes in the chemical, pharmaceutical and food industries.[2] Primarily, it is used as a precursor for the synthesis of the polyamide Nylon-6,6.[1,3] Additionally, AA is widely used for the production of polyester and polyurethane resins, as a plasticizer in the production of polyvinyl chloride (PVC) and polyvinyl butyral (PVB), and as an approved additive in cosmetics, gelatins, lubricants, fertilizers, adhesives, insecticides, paper and waxes.[1,3] In 2013, ~3.5 million metric tons of adipic acid were produced, reflecting a ~5% growth rate per year over the past 5 years.[4] Nearly 95 % of the world wide industrial production of adipic acid employed the nitric acid oxidation method.[4] The first step is air oxidation of cyclohexane, where high temperature (125° - 165°C) and high pressure (8-15 atm) are employed to produce KA oil/"olone" (i.e., a mixture of cyclohexanone and cyclohexanol) with 4 -11% conversion and ~85% selectivity.[4] In the second step, nitric acid is applied as an oxidant: the conversion is ~100%, and the selectivity for adipic acid is 93-95% with some other short-chain acids are produced as side products. Demerits of the current industrial process involve low overall product yield, corrosion of reaction vessels by nitric acid, emission of N_2O, which is ozone-depleting greenhouse gas and finally, high energy consumption. It was estimated that ~0.3 kg of N_2O gas is formed per kilogram of AA produced. After energy-consuming recovery and recycling, the amount of N_2O gas released to the atmosphere still accounts for ~5 to 8% of annual anthropogenic N_2O emission worldwide.[4] Many efforts have been devoted to developing more efficient and environmentally friendly processes for industrial production of AA that devoid N_2O emission.

The hydrogen peroxide-based catalytic conversion has received much attention; it has the high content of active oxygen species (47 wt%) as it generates water as the sole by product.[5] Moreover, H_2O_2 is cheaper and safer to use than the other peroxides and peracids; so many researchers came forward to produce adipic acid by oxidation of cyclohexane, using H_2O_2 as oxidant. The first successful oxidation of cyclohexene to AA was reported in a seminal contribution by Sato et al., who developed a biphasic system using 30% H_2O_2 in the presence of Na_2WO_4 as a homogeneous catalyst and $[CH_3(n\text{-}C_8H_{17})_3N]HSO_4$ as a phase-transfer catalyst.[6] An AA yield of 90% was furnished after 8 h. Freitag et al. then improved this biphasic system using an Na_2WO_4 catalyst and microwave radiation, reducing the reaction time to 90 min with 68% yield.[7] Bohstro¨m et al. demonstrated the conversion of cyclohexene to AA in aqueous dispersions of mesoporous oxides with built-in catalytic WO_3 sites.[8] Several other tungstate-based catalysts have been reported as well, including oxo-tungsten-containing SBA-15,[9] $[BMIm]_2WO_4$ supported on silica sulphamic acid,[10] $H_3PW_{12}O_{40}$[11] and combinations of Na_2WO_4 with H_2SO_4[12] or H_2WO_4 with acidic resins,[13] thus emphasizing the remarkable catalytic efficiency of tungstate in this oxidation reaction. Lee et al. explored titanium framework-substituted aluminophosphate (TAPO-5) as another catalyst for the oxidation of cyclohexene to AA.[14] Chavan et al. have used a Co/Mn cluster complex as a catalyst to convert cyclohexanone to AA in acetic acid medium with a selectivity of 86%.[15] Recently, our group reported conversion of cyclohexene to AA with very high yield (~94%) over silver supported tungsten oxide nanorod catalysts using H_2O_2 as oxidant.[16] Although there are several reports on preparation of AA by various processes from various substrates,[17] Production of AA by direct oxidation of cyclohexane has been rarely reported; moreover, none of the reported processes have been developed, largely because either high reaction temperatures have been employed or poor selectivity of AA was observed, despite higher conversion, or severe leaching of the catalyst was observed. Therefore, there is substantial interest in the development of more efficient, readily separable, reusable catalysts for the catalytic oxidation of cyclohexane.

Supported Cu (II) species employed catalytically in many important reactions[18] and the catalytic properties of the active copper phase can be greatly influenced by the nature of the support and the dispersion of the active component.[19] We reported that Cu (II) nanoclusters supported on nanocrystalline Cr_2O_3 catalyst efficiently converts cyclohexane to cyclohexanone with high yield at room temperature, but the catalyst failed to show any activity in AA production by direct oxidation of cyclohexane, even at drastic condition.[20] In the path of our research, we synthesized Cu (II) nanoclusters supported on nanocrystalline W (VI) oxide with size 25-65 nm in hydrothermal process, promoted by cationic surfactant cetyltrimethylammonium bromide. To our delight, this catalyst accomplished >88% conversion of cyclohexane with >75% AA selectivity by virtue of C_{sp3}-C_{sp3} bond rupture.

2. Experimental

2.1 Materials

Hydrogen Peroxide (50 wt % in water) was purchased from Merck KGaA, Darmstadt, Germany. Ammonium metatungstate, hydrate, anhydrous cupric chloride, cetyltrimethylammonium bromide (CTAB), hydrazine (80% aq. solution), ammonium hydroxide, cyclohexane (purity > 99.9%), acetonitrile (HPLC grade) were purchased from Sigma-Aldrich Co. All the chemicals were used without further purification.

2.2 Synthesis of the catalyst

Cu (II) nanoclusters supported on nanocrystalline WO_3 was prepared modifying our own process, taking $CuCl_2$ and $(NH_4)_6H_2W_{12}O_{40}\bullet xH_2O$ as precursor of Cu and W respectively.[20] In a typical procedure 5. 3 g $(NH_4)_6H_2W_{12}O_{40}\bullet xH_2O$ and 0.40 g of $CuCl_2$ were dissolved in 16 g deionized water. Then the solution was made basic to a pH range of 8 using NH_4OH solution dropwise. After that, a transparent and homogeneous precursor solution formed, 0.8 g CTAB was added into the solution. After the solution has been stirred for half an hour, aqueous hydrazine solution (0.4 g) was added to it. All the reagents were added maintaining the molar ratio: Cu: CTAB: H_2O: N_2H_4 = 1: 0.75: 300: 1. The resulting precursor solution was transferred into a Teflon-lined autoclave with a stainless steel shell. The autoclave was sealed and maintained at 180 °C for 24 h. After cooling naturally to room temperature, the white products were collected after centrifuging, washed sequentially with distilled water and absolute ethanol to remove ions possibly remnant in the products, and dried in an oven at

100°C for overnight. Finally, the white powders were undergone calcinations under oxygen atmosphere at 550°C for 6h to get canary-yellow products (catalyst).

2.2 Catalyst characterization techniques

X-ray power diffraction (XRD): Powder X-ray diffraction patterns were collected on a Bruker D8 advance X-ray diffractometer fitted with a Lynx eye high-speed strip detector and a Cu K_{α} radiation sourceusing Cu Ka radiation with a wavelength of 1.5418 Å. Diffraction patterns in the 2°-80°region were recorded at a rate of 0.5 degrees (2θ) per minute. The resulting XRD profiles were analyzed to identify the crystal phase of the compound using reference standards. The line width of the most intense XRD peak was taken for estimation of crystallite size by the Scherrer equation. Scanning electron microscopy (SEM): Scanning electron microscopy images were taken on a FEI Quanta 200 F, using tungsten filament doped with lanthanum hexaboride (LaB_6) as an X-ray source, fitted with an ETD detector with high vacuum mode using secondary electrons and an acceleration tension of 10 or 30 kV. Samples were analyzed by spreading them on a carbon tape. Energy dispersive X-ray spectroscopy (EDX) was used in connection with SEM for the elemental analysis. The elemental mapping was also collected with the same spectrophotometer. Samples were subjected to scanning electron microscope analysis to understand the shape, size, and morphology properties. Transmission electron microscopy (TEM): The particle size and distribution of the samples were analyzed by TEM, JEOL JEM 2100 microscope, and samples were prepared by mounting an ethanol-dispersed sample on a lacey carbon Formvar coated Cu grid. X-ray photoelectron spectroscopy (XPS): X-Ray photoelectron spectra were recorded on a Thermo Scientific K-Alpha X-Ray photoelectron spectrometer and binding energies (±0.1 eV) were determined. The resulting spectra were analyzed to identify the different oxidation states of the copper and chromium ions present in the sample. Prior to the analysis, the spectra were calibrated with reference to C1s observed at a binding energy of 284.5 eV. Inductively coupled Atomic Absorption Spectroscopy (ICP-AES): Chemical analyses of the metallic constituents were carried out by Inductively Coupled Plasma Atomic Emission Spectrometer; model: PS 3000 uv, (DRE), Leeman Labs, Inc, (USA). Thermogravimetric Analyses (TGA) of the uncalcined catalyst were carried out in a Pyris Diamond, Perkin Elmer Instruments and Technology by SII (Seiko Instruments INC), USA] instrument-balance by heating 2.15 mg samples at 5 °C min^{-1} in flowing air atmosphere. Raman spectra was measured at 298K by using a Laser Raman Spectrometer (JASCO, NRS-3100) with the 532 nm line from a diode-pumped solid-state laser for excitation. Fourier transform infra-red (FT-IR) spectra were recorded on a Thermo Nicolet 8700 (USA) instrument with the operating conditions: resolution: 4 cm^{-1}, scan: 36, operating temperature: 23–25 °C and the frequency range: 4000-400 cm^{-1}. Spectra in the lattice vibrations range were recorded for wafers of sample mixed with KBr.

2.3 Reaction setup

Liquid phase oxidation reaction was carried out in a two neck round bottom flask, equipped with refrigerant, containing 0.1 g catalyst, 10 ml solvent and 1 g benzene to which H_2O_2 (50% aq. solution) was added dropwise to prevent immediate H_2O_2 decomposition. The flask was then emerged in a preheated oil bath and vigorously stirred with a magnetic stirrer. The reaction temperature was ranged between RT and 90 °C. Small aliquots of the sample were withdrawn from the reaction mixture at regular intervals for analysis using a syringe. At the end of the reaction, the solid particles (catalyst) were separated by filtration and the products were analysed by Gas Chromatograph (GC, Agilent 7890) connected with a HP5 capillary column (30m length, 0.28 mm id, 0.25 µm film thickness) and flame ionisation detector (FID). Chem Station software was used to collect and analyze the respective GC-data. The relative error of product determination did not exceed ±5%. The benzene conversion and phenol formation were calculated using a calibration curve (obtained by manual injecting the authentic standard compounds). An anisole solution with a known amount was used as an external standard for analysis. The individual yields were calculated and normalized with respect to the GC response factors. The product identification was carried out by injecting the authentic standard samples in GC and GC-MS. For the reusability test, the catalyst was repeatedly washed with acetonitrile and acetone and dried overnight at 110 °C and used as such, without regeneration. In order to check the metal leaching the mother liqor was then analyzed using ICP-AES.

2.4 Material Balance

We have performed the C-balance for the most of the experiments and have also done the material balance for few experiments. The estimated error in analysis arising due to sampling and handling losses was $\underline{+}$ 5%.

3. Results and discussion

3.1 Generation of CuW Nanoparticles

It is believed that, the precursors of copper and tungsten ionizes and counter ions diffuse into the aqueous solution, maintaining the homogeneity of the medium. When concentration of the micelles was less than that of critical micelle concentration (CMC), Cu^{2+} and W^{6+} ions (hydrated) are preferentially located at the micellar surface due to presence of Br^{-} ions.[22] The growth of the particles occurs along the side of the particles, which is exposed to water. When concentration of the surfactant becomes $\geq$ CMC, the aqueous medium is largely populated by surfactant micelles. The Cu and W-precursor ions approach towards the micellar headgroup region. In this situation, growth of the particles in a particular direction is prohibited due to the micellar steric effects and the nanoparticles are allowed to grow to form spherical nanoparticles with limited size. Basic medium influences the role of CTAB and hydrazine prohibits Ostwald ripening process to a certain extent.[23]

3.2 Catalyst characterization

The X-ray diffraction analyses (XRD) of the catalyst was carried out to determine the crystallite phase of the Cu-W nanocomposites as shown in Fig. 1. Sharp peaks at $2\theta = 23.1^\circ$, 23.7°, 24.4°, 33.3° and 34.0°, confirm the formation of monoclinic WO_3 (JCPDS No. 43-1035, space group: P21/n). In addition, XRD reflections with comparatively low peak strength due to crystalline CuO (monoclinic) were also noticed at $2\theta = 35.57^\circ$, 38.75°, 48.7°, 68.2° etc. [JCPDS card no. 89-2530]. Applying Debye-Scherrer equation, the average crystallite sizes of the particles was determined to be 48 nm (based on $2\theta = 23.1^\circ$) which is actually near the size of the crystallites as seen under HRTEM imaging. Moreover, other crystalline by-products or other phases of copper/tungsten oxides were not detectable by XRD, indicating the high purity of our synthetic procedure.

XPS was utilized to detect the surface composition and the chemical state of the catalyst. The XPS binding energies (BE) of some characteristic core levels of Cu and W in the Cu-W samples have been presented (Fig. 2 & 3 respectively). The Cu 2p XPS results indicate that the binding energy of the Cu 2p electron in the sample, and the peaks center at approximately 935.7 eV corresponding to $Cu2p_{3/2}$.[24] The existence of satellite peaks in the spectra suggests that copper exists in the samples as Cu (II). The value of the binding energy (~935.7 eV) is much greater than that of pure CuO (933.8 eV), which indicates that the Cu (II)-species are surrounded by tungsten oxide. The W $4f_{5/2}$ and $4f_{7/2}$ spectra attributed to the binding energies 37.9 eV and 35.8 eV respectively suggesting that the tungsten in the tungsten oxide sample exists as W^{+6}.[16, 25] XRD and XPS data support the fact that, the main phase is comprised of monoclinic W (VI) oxide and the supported metal is of Cu (II) oxide.

To further investigate the surface property and to detect subtle phase information of the composite, we conducted Raman (Fig. 4) and FTIR-spectrum (Fig. 5) analyses of the sample. Generally, the 950–1050 cm^{-1} Raman wavenumbers of the transition metal oxide are assigned to be the symmetric stretching modes of metal and oxygen bonds [short terminal W=O, υ_s(W= O) terminal bands], and 750–950 cm^{-1} bands were either the antisymmetric stretching of W–O–W bonds [υ_s(W–O–W)] or symmetric stretching of–O–W–O– bonds [υ_s(–O–W–O–)].[26] The Raman spectrum of the Cu/WO_3 NP catalyst detected vibrational peaks at 806, 718, 686, 326, 274, 134, 76 and 60 cm^{-1}. The two main intense peaks at 806 and 718 cm^{-1}, and the shoulder at 686 cm^{-1}, are typical Raman peaks of crystalline WO_3, which correspond to the stretching and bending vibrations of the bridging tungsten and oxygen atoms.[26] They are assigned to be the W–O stretching (υ), W–O bending (δ) and O–W–O deformation (γ) modes, respectively. Two peaks at 326 and 274 cm^{-1} are assigned to be the bending δ(O–W–O) vibrations.[26] Those below 200 cm^{-1} modes were attributed to the lattice vibrations.[26]

This assignment is tentative and requires further confirmation by FTIR measurements (Fig. 5). The peaks of the uncalcined sample at 812, 1062 cm^{-1} can be assigned to the C-N^+ stretching modes of CTAB molecules.[26d,27] The peak at 1378 and at 1462 cm^{-1} are assigned to symmetric mode of vibration of the head groups of the methylene moiety (N^+—CH_3) and CH_2 scissoring mode respectively.[2] The frequencies above 1600 cm^{-1} to 3000 cm^{-1} are due to CH_2 symmetric and antisymmetric vibrations, respectively. It is to be noted that, the shift of vibrations to lower frequency occurred as the alkyl chains experienced a more hydrophobic environment in Cu-W blocks upon the surface of which the CTA-moieties were supposed to be bound.[26d] It can be inferred that, the mutual interactions between CTAB and the Cu-W surface have taken place. Some bands were detected at 2800–3020 cm^{-1}, which can be attributed to the CTAB surfactant. The FTIR spectrum of CTAB shows two intense bands at 2918 and 2846 cm^{-1}, corresponding to the asymmetric and symmetric stretching vibrations of C–CH in the methylene chains. The sharp bands at 1450–1500 cm^{-1} were specified as the deformation of –CH_2– and –CH , and the weak band at 3011 cm-^{1} as the C–CH_3 asymmetric stretching and N–CH symmetric stretching vibrations of the solid surfactant.[26d] These typical frequencies were absent when the material was calcined at 500 °C in air (fresh catalyst) in the case of the prepared catalyst, which indicated that, the embedded CTAB moieties have been completely removed from the catalyst surface during calcination. In the crystalline structure of WO_3, W atoms are located in the centre of WO_6 octahedra with O at the vertices forming W-O-W connections.[28] For such an arrangement, the IR active bands are fundamental vibrations of W=O, W-O and W-O-W. These can be stretching (υ) or in-plane bending vibrations (δ) and out-of-plane wagging (γ).[29] The main WO_3 vibrations are found in the 1700–380 cm^{-1} IR region. All synthesis temperatures present characteristic peaks at 570, 800, 895, 964, 1045, 1404 and 1608 cm-^{1} associated with γ(W-O-W), υ(W-O-W), υ(W-O-W), υ(W-O, W=O), δ(W-OH), υ(OH) and δ(OH) in W-OH respectively. The -OH bands are associated with surface hydroxyl groups and weakly bound solvent, ethanol/water. A stronger broad band around 3350 cm^{-1} should appear from a W-OH mode if intercalation of H_2O had occurred.[29] The band at 517 cm^{-1} is also marked with asymmetric line broadening indicating the presence of a band at 500 cm^{-1}, which is the characteristic band of Cu–O. The three absorption peaks at 601, 508 and 432 cm^{-1} are assigned to the A_u mode and $2B_u$ modes, respectively. The peak at 601 cm^{-1} is likely to be from Cu-O stretching along the [¯101] direction and the peak at 508 cm^{-1} is likely to arise from Cu-O stretching along the [101] direction.[30] Moreover, it was also confirmed from the FTIR diagram that, there was no structural deformation in the catalyst even after 4 recycles.

The topology of the catalyst was studied by scanning electron microscopy (SEM, Fig. 6) which showed a typical sample composed of throughout uniform spherical pea-shaped nanoparticles in the range of 35-65 nm. SEM images revealed that, all the nanoparticles organized into spherical assemblies, owing to the structure directing effect of the template. SEM-EDX analysis of the composite revealed that, there appears a distribution of Cu, W and O only, and no sort of C or Br, which are visualized from the SEM-EDX image of the uncalcined sample (Fig. S1, ESI†). This observation indicated the complete removal of the structure-directing template (s). This experimental finding was further supported from TGA analysis of the unalcined catalyst (Fig. S2, ESI†). It was also speculated from SEM diagram that, increment in Cu loading spoils the uniformity of the samples and the particle size of the catalyst also increases (Fig. S3, ESI†).

However, transmission electron microscopy (TEM) image revealed that the sample is comprised of several spherical pea-shaped particles (Fig. 7) with 55 nm in size in average. To get further information about the catalyst structure, a representative high resolution TEM (HRTEM) image taken from a nanoparticle is shown in Fig.7c. The lattice fringes with a d-spacing of 0.23 nm, corresponding to the spacing of the [111] planes of monoclinic CuO is conveniently discriminated from that of the [020] planes of monoclinic WO_3 with a d-spacing of 0.30 nm .[16,24,31] Typically, the dispersion of Cu, W and O atoms in the catalyst were also analyzed by STEM-elemental mapping (Fig. 8). It indicated that each of Cu, W and O species was homogeneously dispersed.

The UV–vis absorbance for Cu/WO_3 NP catalyst (Fig. 9) shows an absorption band in the 200–450 nm. No absorption band in the visible range was detected. The charge-transfer (CT) bands give us an idea of the environment in the neighborhood of Cu^{2+} ions. According to the literature, the band at 210-270 nm indicates the O ligand-to-metal charge-transfer (LMCT) transition, where the Cu ions occupy isolated sites over the support. The band at 355 nm indicates the formation of (Cu-O-Cu) clusters in a highly dispersed state, which is not detectable by XRD.[24]

The corroboration of all the catalyst-characterization data led to the conclusion that, the main phase of the catalyst is comprised of monoclinic W (VI) oxide, whereas a small amount of CuO is dispersed (as active component) on this phase of the catalyst surface.

3.3 Catalytic activity

Table 1 shows the catalytic activity of differnt catalysts in direct AA production from cyclohexane. Blank reaction was performed (Table 1, entry 1) and we noticed very poor conversion of cyclohexane with cylohexanone as the only product. This indicated the necessity of catalyst. Notably, commercial CuO and WO_3 catalyst did not show any activity (Table 1, entry2, 3). Conventional catalyst prepared by impregnation method also showed negligible activity (Table 1, entry 4). The poor catalytic activity of the impregnated catalyst may be attributed to their irregular shape and larger particle size, which limits the accessibility of the catalyst towards the reacting substrates. We introduced our so prepared Cu/WO_3 nanoparticles catalyst and we noticed 66% yield of AA. Various reaction parameters that regulated the yield of AA were studied (like temperature, time etc.). It was found that temperature has prominent effect on cyclohexane conversion. The catalyst showed negligible conversion at RT but with increasing temperature, the conversion of cyclohexane increased rapidly (Fig. 10), possibly because initially produced cyclohexanol, cyclohexanone and cyclohexane diol were compelled to undergo further reaction to produce AA. 70 °C was proved to be the optimum reaction temperature. With further increment in temperature (90°C), we noticed that, conversion of cyclohexane decreases, probably due to the fact that, H_2O_2 decomposes rapidly in this temperature. When cyclohexane : H_2O_2 molar ratio was low (1: 1), we noticed very poor conversion of cyclohexane. The optimum cyclohexane : H_2O_2 molar ratio was proved to be 1: 3; increment of H_2O_2 concentration (Fig. 11) lead to the decrement in AA yield, probably due to the fact that, decomposition of H_2O_2 produced excess water in the reaction mixture and thereby contact of cyclohexane (immiscible in water), catalyst and H_2O_2 (highly soluble in water) is interrupted. Maintaining all the optimum reaction conditions, when the reaction was allowed to run for hours (Fig.12), we noticed increment of AA yield with time. After 12h, we didnot notice any appreciable increment of AA yield reflecting the fact that the unreacted H_2O_2 decomposed after 12h.

It was also noticed that, higher loading of Cu decreased the yield of AA, probably due to the fact that loading of Ag lead to the formation of Ag-agglomerates (as confirmed from SEM diagram, Fig S3, ESI†), that decreased the active metal dispersion and catalyst-efficacy.

In the light of the above experimental findings, we can draw the hypothesis that, Cu (II) is the reactive species in the catalyst and the reaction proceeds through free-radical mechanistic pathway. We believe that, Cu (II) in the catalyst framework interacts with the C–H bond of cyclohexane and probably, the flexibility property of the Cu (II)-framework renders the catalytic system suitable for lowering the activation energy of the oxidation reaction. At normal condition, H_2O_2 does not interact with cyclohexane. H_2O_2 dissociation is believed to occur homogeneously over Cu/WO_3 nanoparticles catalyst and follows the mechanism proposed by Kazarnovsky.[33] Dissociation of H_2O_2 over the catalyst generates active •OH free radicals that are stabilized by the solvent acetonitrile to a great extent.[34] The electronegativity of C is 2.55 and that of H is 2.2. Relatively, electron density is accumulated near C-atom rather than H atom. We believe that, the negative charge density generated on C-atom is localized by Cu (II) species present in the catalyst. The generated •OH radicals behave as electrophiles and proceed towards the C-atom bearing partial negative charge.[35] Consequently, a homolytic cleavage of the C–H bond occurs to form cyclohexyl radicals. The concomitantly formed cyclohexyl radicals react with excess •OH radicals to produce cyclohexanol and the latter gets oxidized to form cyclohexanone and cyclohexanediol over the catalyst surface. In presence of excess H_2O_2, the C_{sp2}-C_{sp2} bond rupture takes place and AA is produced (Scheme 1).[36]

Commercial CuO or WO_3 and even CuO supported on WO_3 prepared by impregnation method (Fig. S4, ESI†) didnot show any appreciable activity in oxidation of cyclohexane to AA. These experimental findings can be attributed to the large and non-uniform and irregular shapes of these catalysts, which limit their catalytic activities. Moreover, nanoclusters of Cu(II) oxide supported on nano-crystalline WO_3 prepared in our method showed extraordinary performance in formation of AA from cyclohexane, owing to the synergistic interaction displayed between these two species in the catalyst.

3.4 Reusability test

At the end of the reaction, the catalyst was filtered in the hot condition and was the resulting filtrate was independently analyzed by inductively coupled plasma (ICP) (and atomic absorption spectroscopy for free or dissolved metal ions. Only trace amounts of Cu^{2+} (<3 ppb) were detected; which indicated the fact that, the catalyst is almost devoid of leaching properties; this may be attributed by the fact that, Cu^{2+} remains strongly anchored upon WO_3 support. Recycling and reusability of the catalyst was examined by introducing the used catalyst subsequently 4 times to carry out the catalytic oxidation. The reusability of the catalyst was studied without regeneration of the catalyst in the same experimental condition. Before each recycle, the catalyst was recovered facilely from the reaction mixture (after 6h) by centrifugation, repeatedly washed with ethanol and acetone and kept for drying at 120 °C for overnight. The catalyst did not show any significant loss in its activity even after 4 successive runs (entry 6, Table 1 & Fig. 13) and the catalyst was proved to be truly of heterogeneous nature.

Acknowledgements

SSA and SG thank CSIR and UGC, New Delhi, India, for their respective fellowships. R.B. thanks CSIR, New Delhi, for financial support in the form of the 12 FYP Project (CSC- 0125, CSC- 0117). The Director, CSIR-IIP is acknowledged for his help and encouragement. The authors thank ASD Division, IIP for the analytical services. We gratefully acknowledge Ms. Nishita Lucas, CSIR-NCL, Pune (India), for performing Raman spectroscopy analyses.

References

1. M. T. Musser, Adipic Acid, Ullmann's Encyclopedia of Industrial Chemistry, 2000, DOI: 10.1002/14356007.a01_269.
2. Adipic Acid: A Global Strategic Business Report, 2012, Global Industry Analysts, Inc., USA. Available electronically at http://www.strategyr.com/adipic_acid_market_report.asp.

3. A. Castellan, J. C. J. Bart and S. Cavallaro, *Catal. Today*, 1991, **9**, 237.
4. K. C. Hwang and A. Sagadevan, *Science*, 2014, **346**, 1495.
5. K. Kamata, K. Yonehara, Y. Nakagawa, K. Uehara and N. Mizuno, *Nat. Chem.,* 2010, **2**, 478.
6. K. Sato, M. Aoki and R. Noyori, *Science*, 1998, **281**, 1646.
7. J. Freitag, M. Nüchter and B. Ondruschka, *Green Chem*., 2003, **5**, 291.
8. Z. Bohström, I. Rico-Lattes and K. Holmberg, *Green Chem.,* 2010, **12**, 1861.
9. C.Y. Cheng, K.J. Lin, M. R. Prasad, S. J. Fu, S.Y. Chang, S. G. Shyu, H.S. Sheu, C. H. Chen, C. H. Chuang and M.T. Lin, *Catal. Commun.,* 2007, **8**, 1060.
10. M. Vafaeezadeh, M. M. Hashemi and M. Shakourian-Fard, *Catal. Commun.,* 2012, **26**, 54.
11. K. Fujitani, T. Mizutani, T. Oida and T. Kawase, *J. Oleo Sci.*, 2009, **58**, 37.
12. P. Jin, Z. Zhao, Z. Dai, D. Wei, M. Tang and X. Wang, *Catal. Today*, 2011, **175**, 619.
13. H. Wei, H. Li, Y. Liu, P. Jin, X. Wang and B. Li, *ACS Appl. Mater. Interfaces*, 2012, **4**, 4106.
14. S. O. Lee, R. Raja, K. D. M. Harris, J. M. Thomas, B. F. G. Johnson and G. Sankar, *Angew. Chem.,* 2003, **42**,1520.
15. S. A. Chavan, D. Srinivas and P. Ratnasamy, *J. Catal.,* 2002, **212**, 39.
16. S. Ghosh, S. S. Acharyya, S. Adak, L. N. S. Konathala, T. Sasaki, and R. Bal, *Green Chem.,* 2014, **16**, 2826.
17. S. V. de Vyver and Y. Roma´n-Leshkov, *Catal. Sci. Technol.*, 2013, **3**, 1465.
18. (a) V. Z. Fridman and A. A. Davydov, *J. Catal.*, 2000, **195**, 20; (b) T. W. Kim, M. W. Song, H. L. Koh and K. L. Kim, *Appl. Catal. A*, 2002, **210**, 35; (c) G. Centi and S. Perathoner, *Appl. Catal. A*, 1995, **132**, 179. (d) M. Matsuoka, W. Ju, K. Takahashi, H. Yamashita and M. Anpo, *J. Phys. Chem. B*, 2000, **104**, 4911.

19. K. I. Choi and M. A. Vannice, *J. Catal.*, 1991, **131**, 22.
20. B. Sarkar, P. Prajapati, R. Tiwari, R. Tiwari, S. Ghosh, S. S. Acharyya, C. Pendem, R. K. Singha, L. N. S. Konathala, J. Kumar, T. Sasaki and R. Bal, *Green Chem.,* 2012, **14**, 2600.
21. S. S. Acharyya, S. Ghosh, R. Tiwari. B. Sarkar, R.K. Singha, C. Pendem, T. Sasaki and R. Bal, *Green Chem.,*2014, **16**, 2500.
22. S. De and S. Mandal, *Colloids Surf., A*, 2013, **421**,72.
23. S. S. Acharyya, S. Ghosh, S. Adak, T. Sasaki and R. Bal, *Catal. Sci. Technol.,*2014, **4**, 4232.
24. K. V. R. Chary, G. V. Sagar, D. Naresh, K. K. Seela and B. Sridhar *J. Phys. Chem. B*, 2005, **109**, 9437.
25. (a) F. Wang, J. Xu, X. Q. Li, J. Gao, L. P. Zhou and R. Ohnishi, *Adv. Synth. Catal.,* 2005, **347**, 1987; (b) S. Ghosh, S. S. Acharyya, D. Tripathi and R. Bal, *J. Mater. Chem. A,* 2014, **2**,15726.
26. (a) M. F. Daniel, B. Desbat, J. C. Lassegues, B. Gerand, M. Figlarz, *J. Solid State Chem.,* 1987, **67**, 235; (b) C. Santato, M. Odziemkowski, M. Ulmann, and J. Augustynski, *J. Am. Chem. Soc.,* 2001, **123**, 10639; (c) I. M. Szilágyi, J. Madarász, G. Pokol, P. Király, G. Tárkányi, S. Saukko, J. Mizsei, A. L. Tóth, A. Szabó, K. Varga-Josepovits, *Chem. Mater.,* 2008, **20**, 4116; (c) O. Yayapao, T. Thongtem, A. Phuruangrat, S. Thongtem, *J. Alloys and Compounds*, 2011, **509**, 2294.
27. (a) W. Cheng, S. Dong and E. Wang, *Langmuir,* 2003, **19**, 9434; (b) S. S. Acharyya, S. Ghosh and R. Bal, *ACS Appl. Mater. Interfaces* 2014, **6**, 14451.
28. M. Gimeno-Fabra, P. Dunne, D. Grant, P. Gooden and E. Lester, *Chem. Eng. J.,* 2013, **226**, 22.

29. (a) I. Hargitta, M. Hargitta, V. Spiridon, E. V. Erokhin, *J. Mol. Struct.,* 1971, **8**, 31; (b) J. Pfeifer, G. F. Cao, P. Tekulabuxbaum, B. A. Kiss, M. Farkasjahnke, K. Vadasdi, *J. Solid State Chem.*, 1995, **119**, 90.
30. K. Kliche and Z. V. Popovic, *Phys. Rev. B: Condens. Matter,* 1990, **42**, 10060.
31. S. S. Acharyya, S. Ghosh and R. Bal, R. *Chem. Commun.* 2014, **50**, 13311.
32. E. Roduner, W. Kaim, B. Sarkar, V.B. Urlacher, J. Pleiss, R. Gläser, W.D. Einicke, G.A. Sprenger, U. Beifuß, E. Klemm, C. Liebner, H. Hieronymus, S.F. Hsu, B. Plietker, S. Laschat, *ChemCatChem*, 2013, 5, 82.
33. I. A. Kazarnovsky, Dokl. AN SSSR, vol. 221, 1975. S353 (in Russian).
34. S.S. Acharyya, S. Ghosh, R. Bal, *Chem. Commun*, 2014, **50**, 13311.
35. S. S. Acharyya, S. Ghosh, S. Adak, D. Tripathi, and R. Bal *Catal. Commun.,* 2015, 59, 145.
36. A. Corma and H. Garci´a, *Chem. Rev.,* 2002, **102**, 3837.

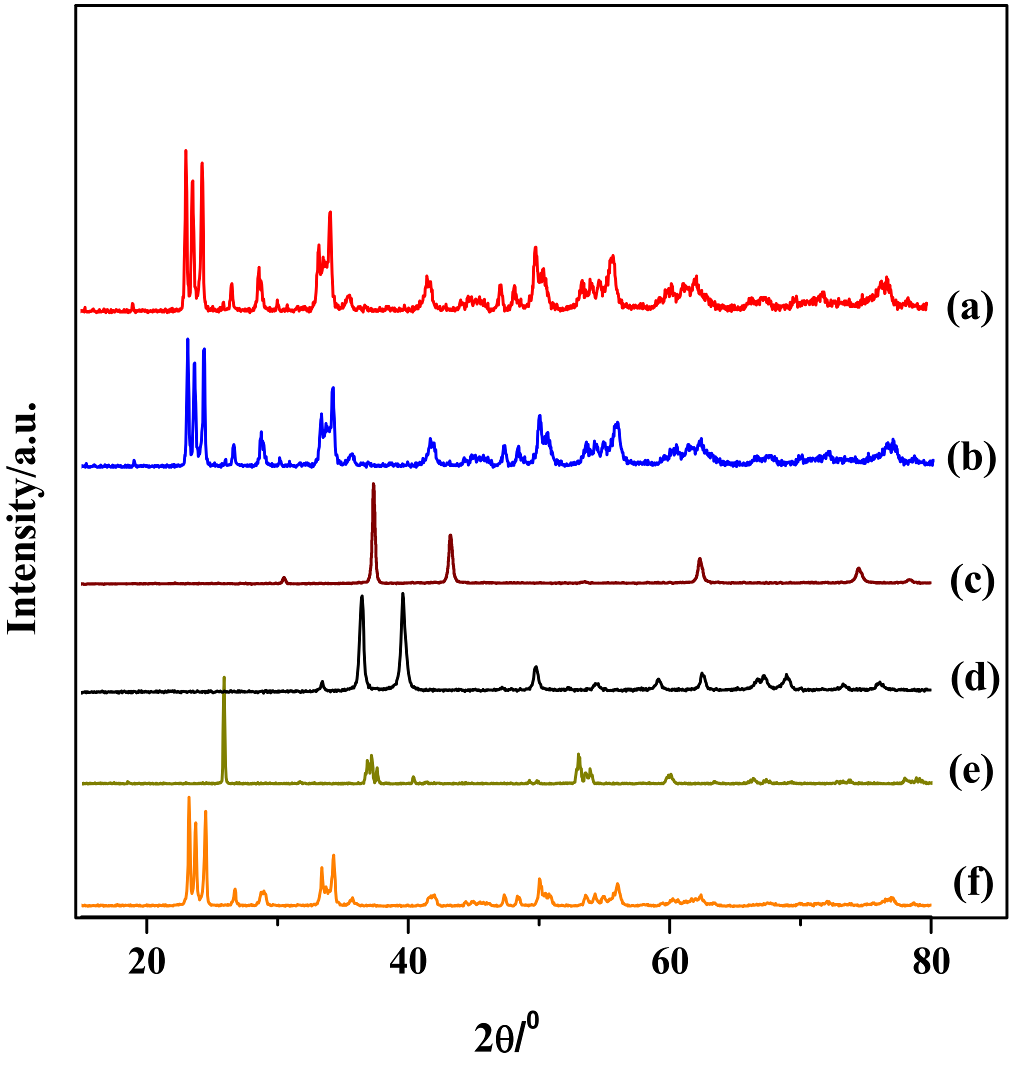

Fig. 1 XRD diffractogram of (a) fresh and (b) spent (after 4 recycles) Cu/WO_3 nanoparticles catalyst and that of (c) commercial Cu (I) oxide, (d) commercial Cu (II) oxide, (e) commercial W (IV) oxide, and (f) commercial W (VI) oxide.

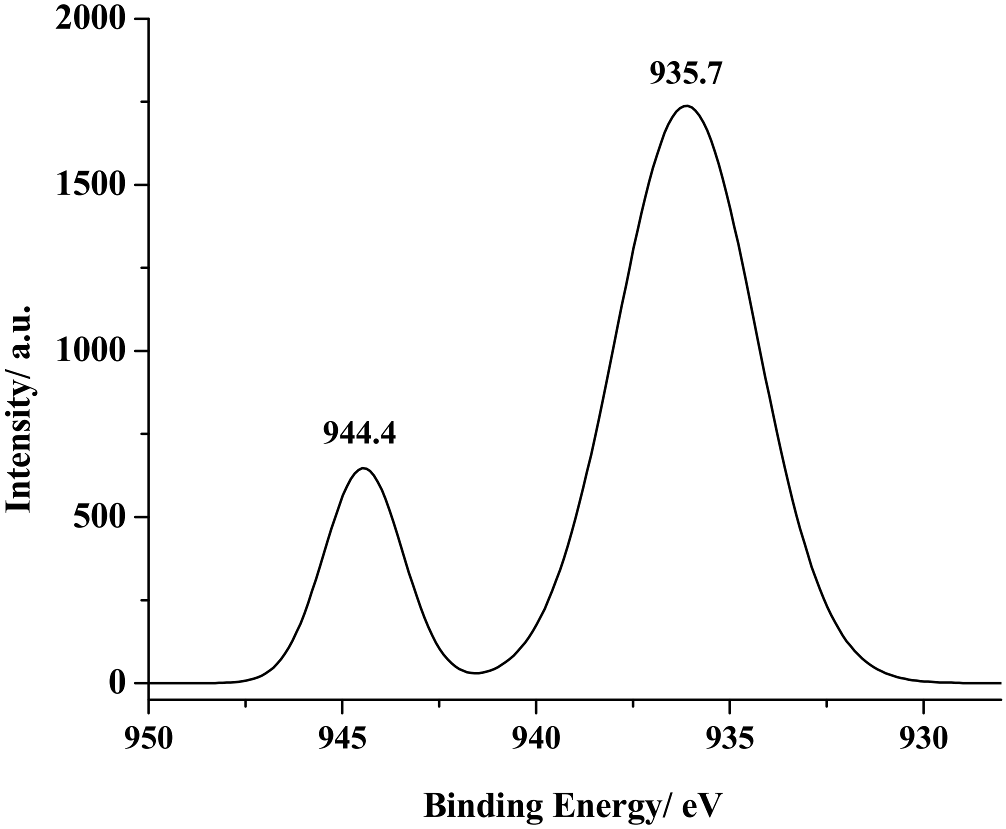

Fig. 2 Cu $2p_{3/2}$ core-level spectra of fresh Cu/WO_3 nanoparticles catalyst.

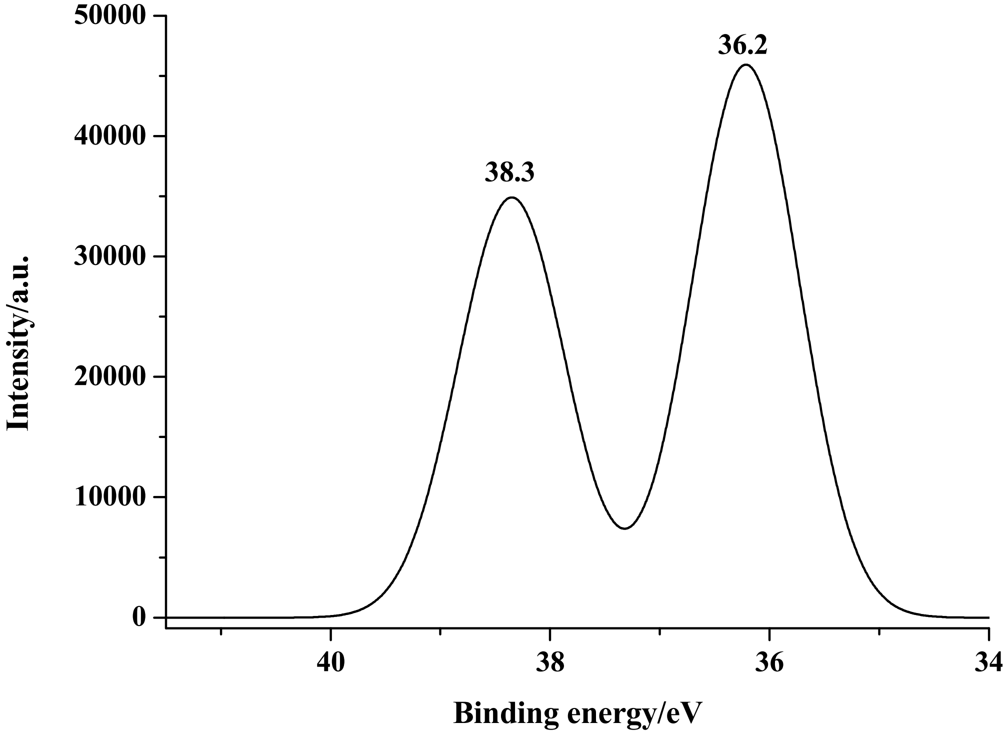

Fig. 3 W4$f_{7/2}$ and W4$f_{5/2}$ core-level spectra of fresh Cu/WO_3 nanoparticles catalyst.

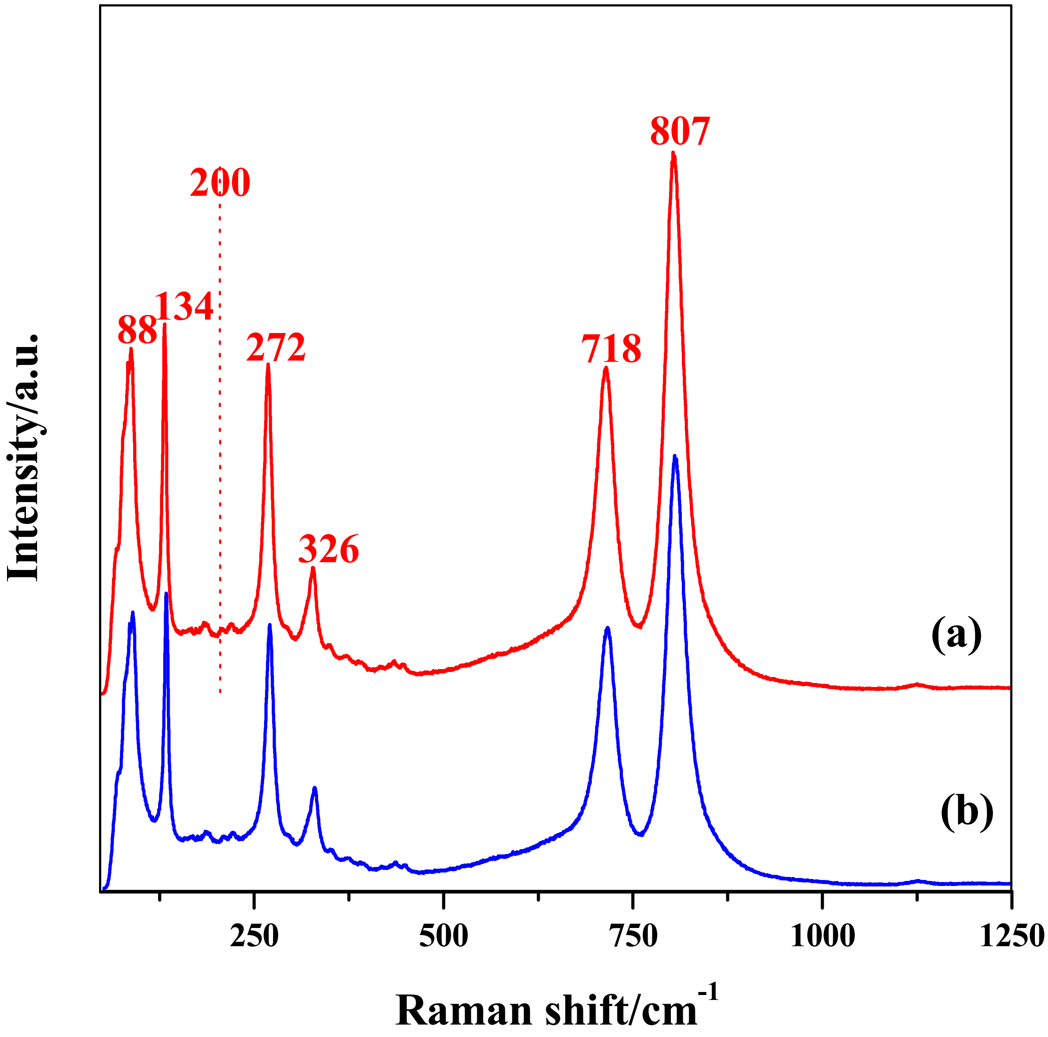

Fig. 4 Raman diagram of (a) fresh and (b) spent Cu/WO_3 nanoparticles catalyst.

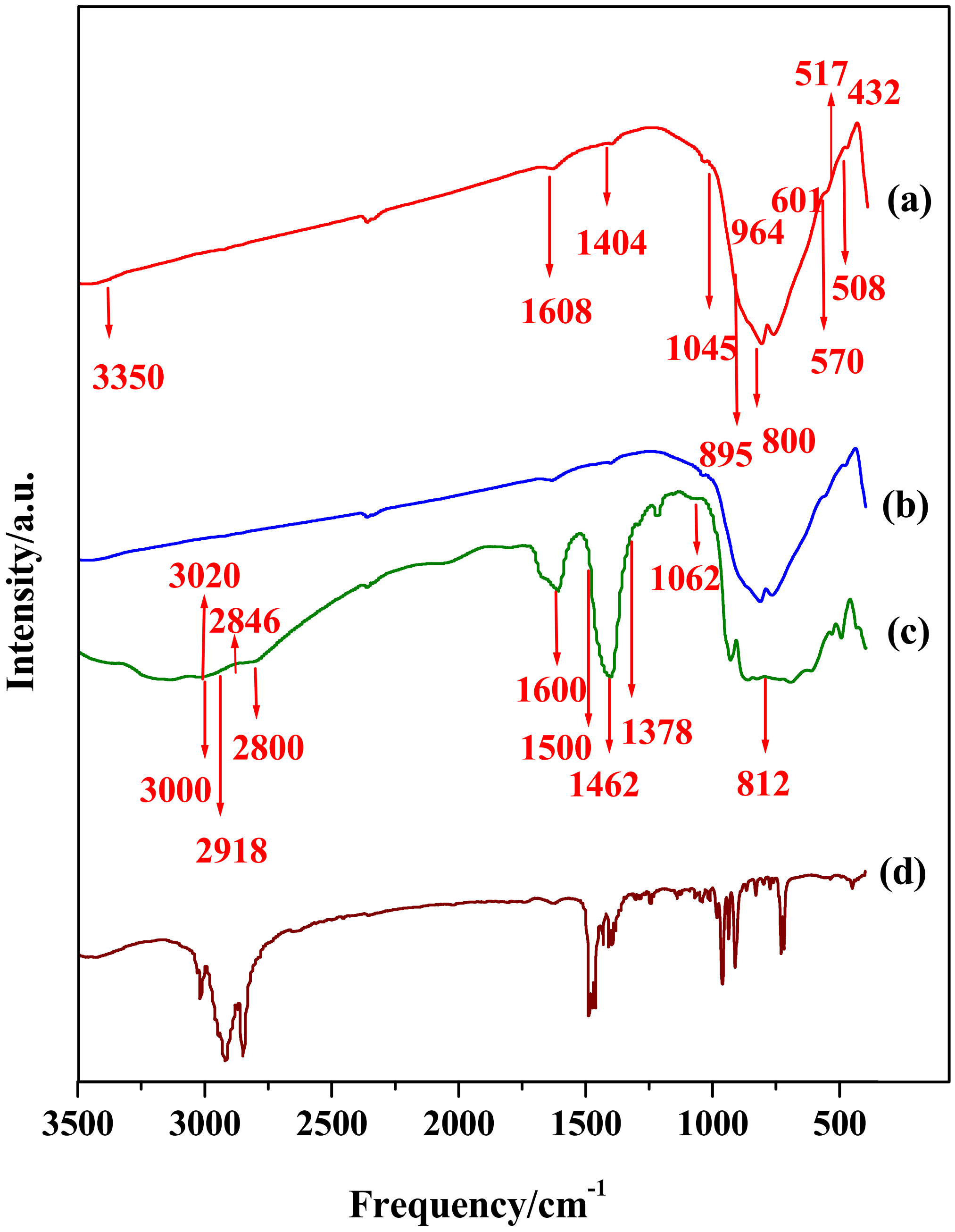

Fig. 5 FTIR diagram of (a) fresh and (b) spent (c) uncalcined Cu/WO_3 nanoparticles catalyst and (d) that of CTAB surfactant.

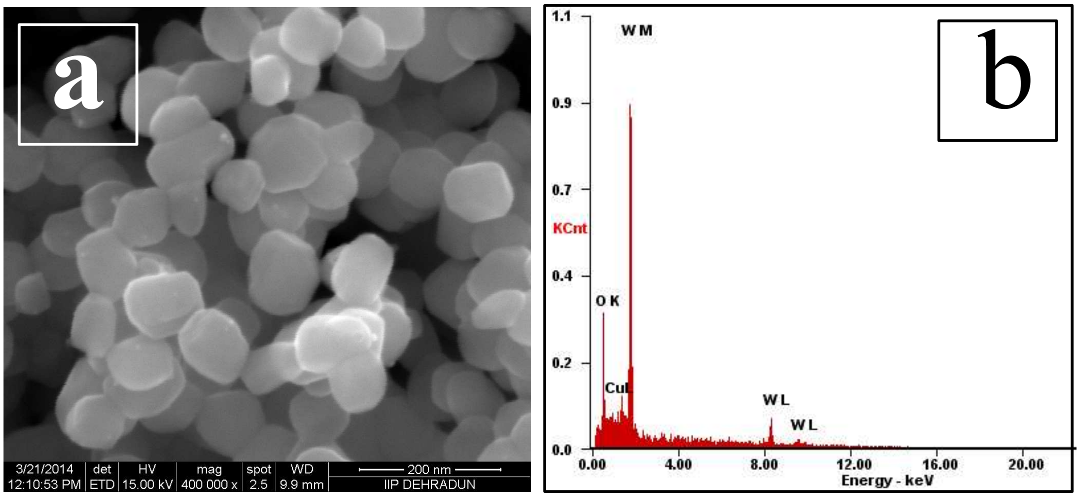

Fig. 6 (a) SEM image and (b) SEM-EDAX image of Cu/WO_3 nanoparticles catalyst.

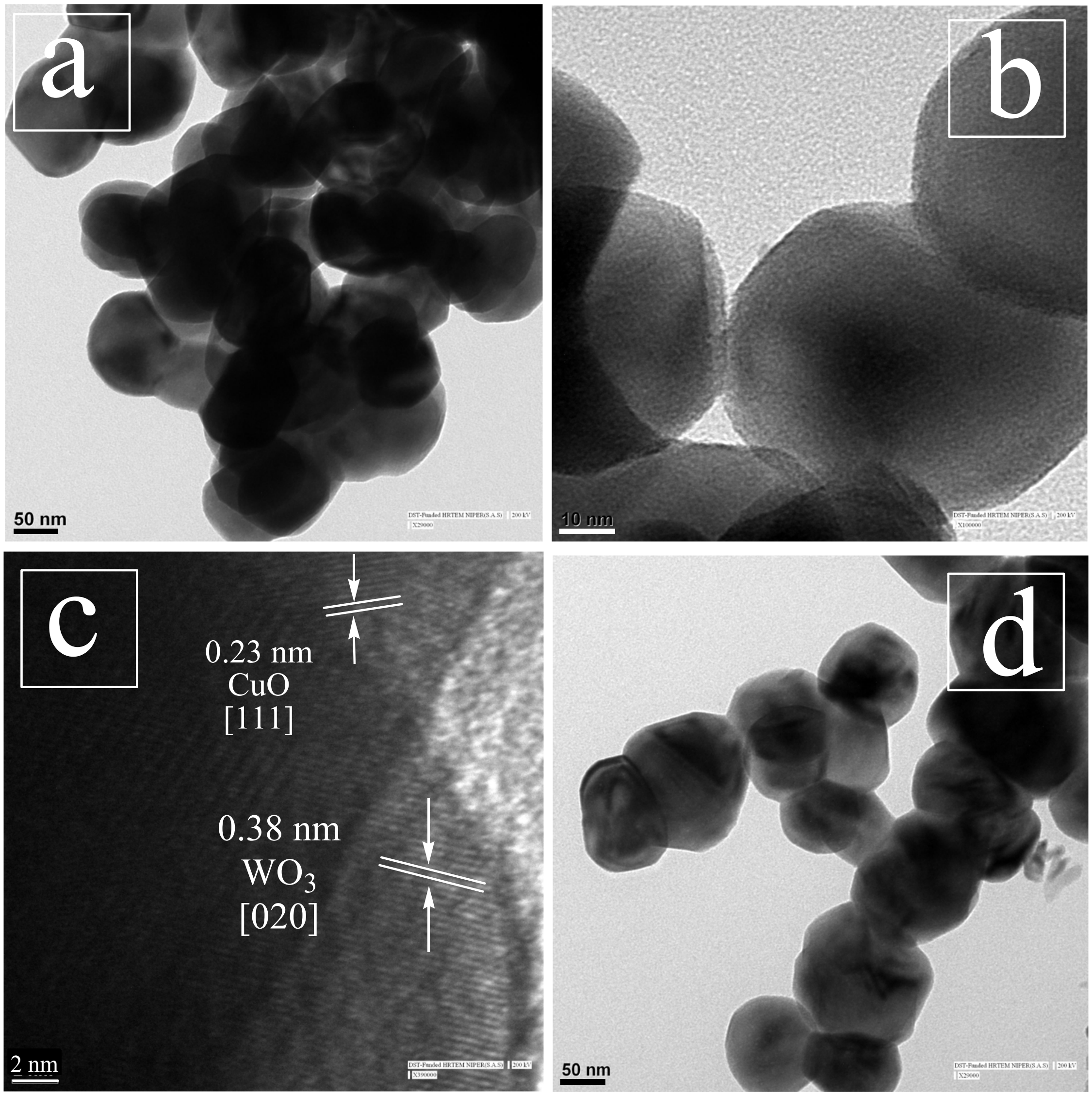

Fig. 7 TEM image of (a-c) fresh and that of (d) spent Cu/WO_3 nanoparticles catalyst.

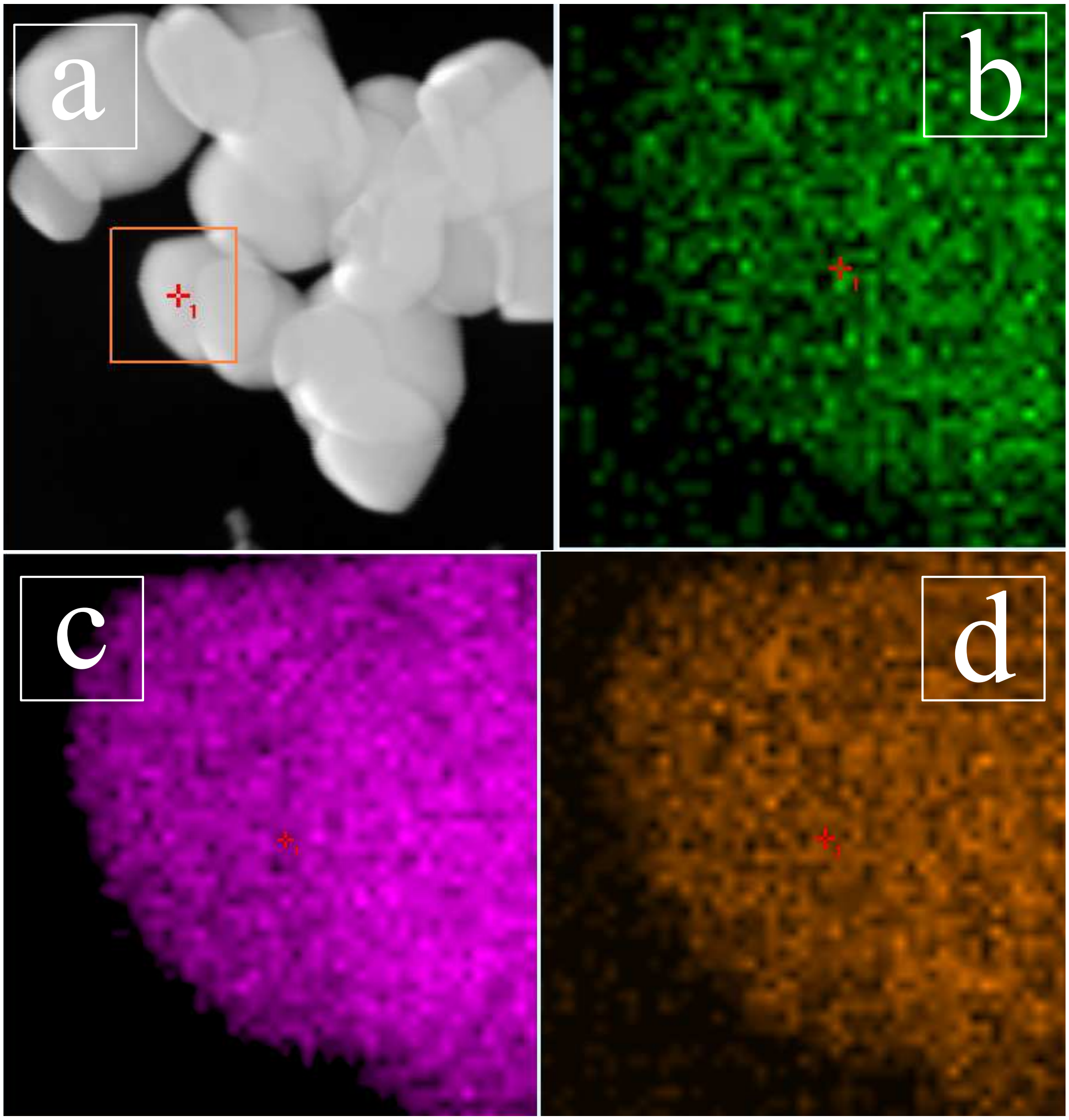

Fig. 8 (a) STEM image and STEM-elemental mapping of (b) Cu, (c) W and (d) O atoms in the fresh Cu/WO_3 nanoparticles catalyst.

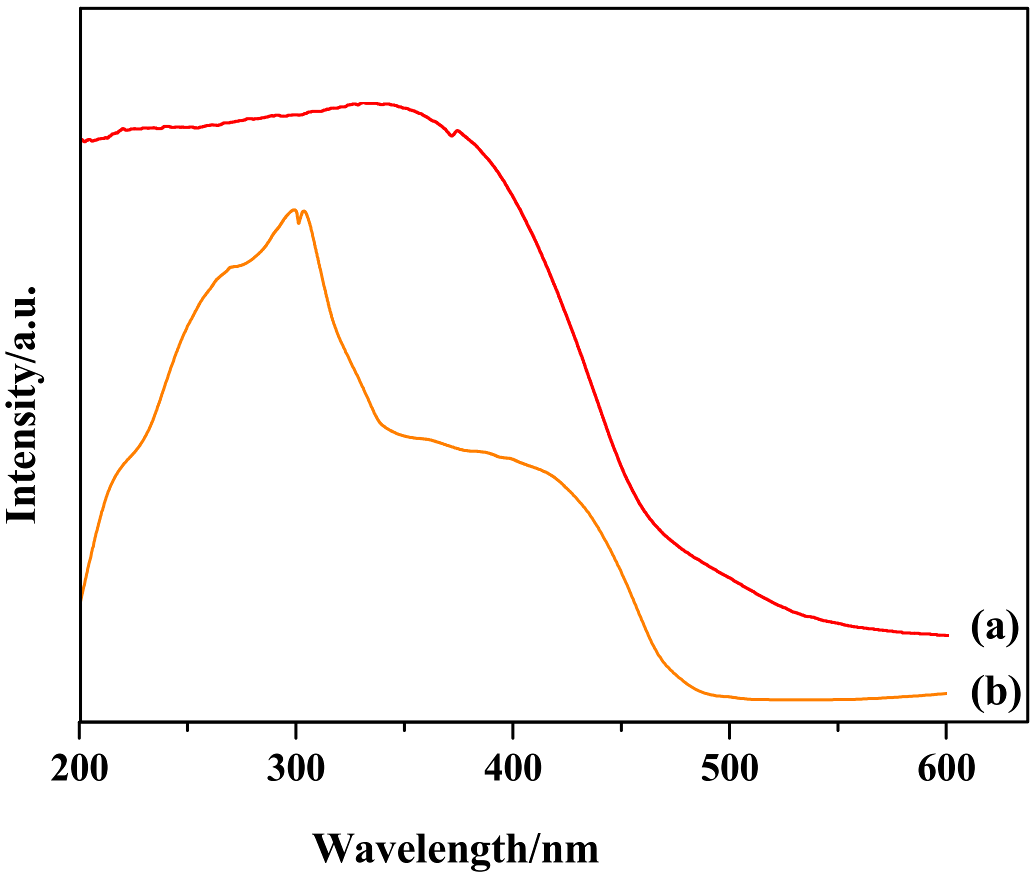

Fig. 9 UV-visible diagram of (a) Cu/WO_3 nanoparticles catalyst and (b) commercial WO_3.

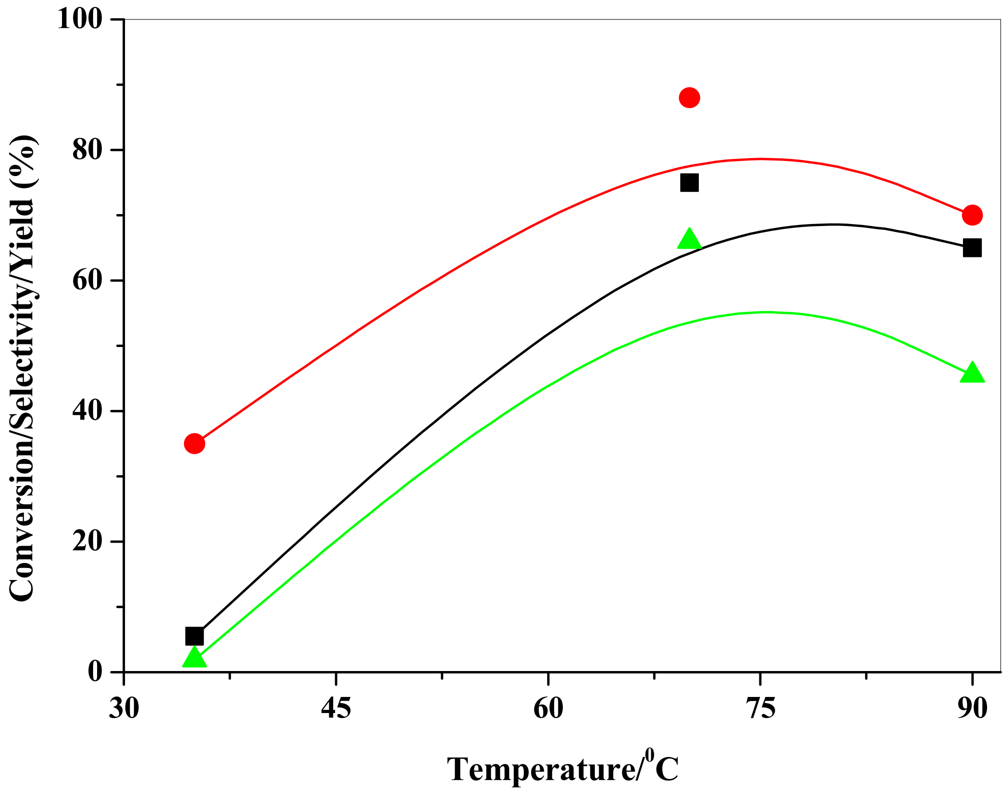

Fig. 10 Effect of temperature on cyclohexane oxidation.
[■] Conversion of toluene; [●] Selectivity to AA; [▲] Yield of AA;
Reaction Condition: cyclohexane =1g; catalyst = 0.15g; cyclohexane: H_2O_2 molar ratio =1:3; time= 12 h.

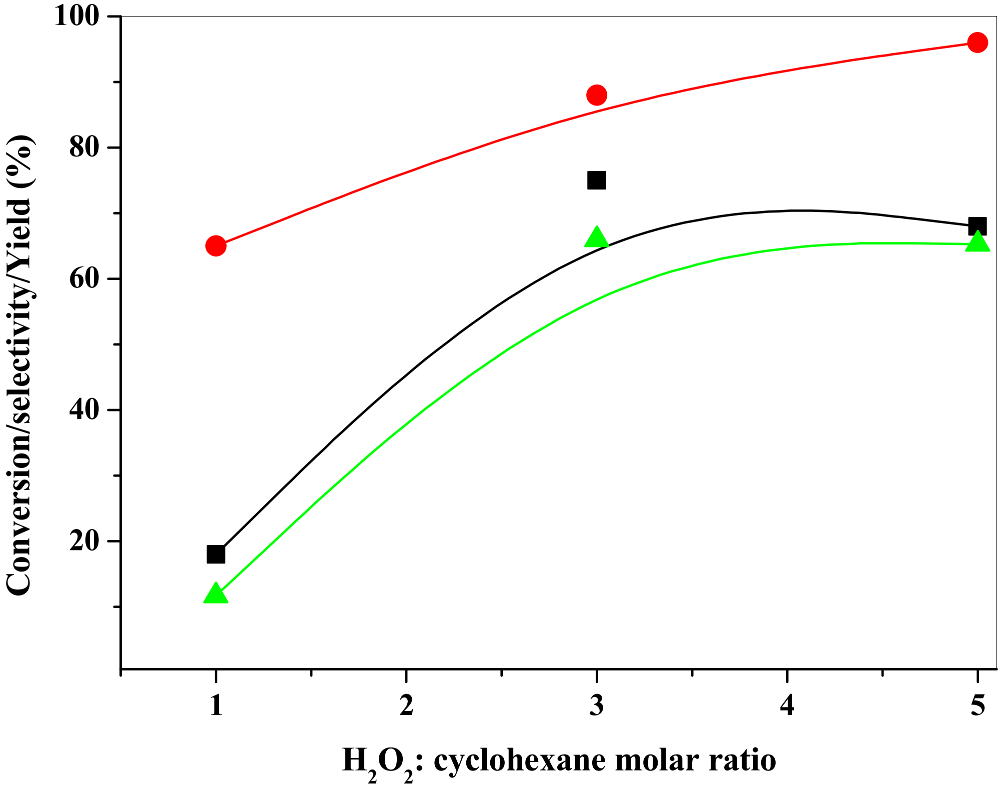

Fig. 11 Effect of H_2O_2 : cyclohexane molar ratio on cyclohexane oxidation.
[■] Conversion of toluene; [●] Selectivity to AA; [▲] Yield of AA;
Reaction Condition: cyclohexane =1g; catalyst = 0.15g; temperature = 70 °C; time= 12 h.

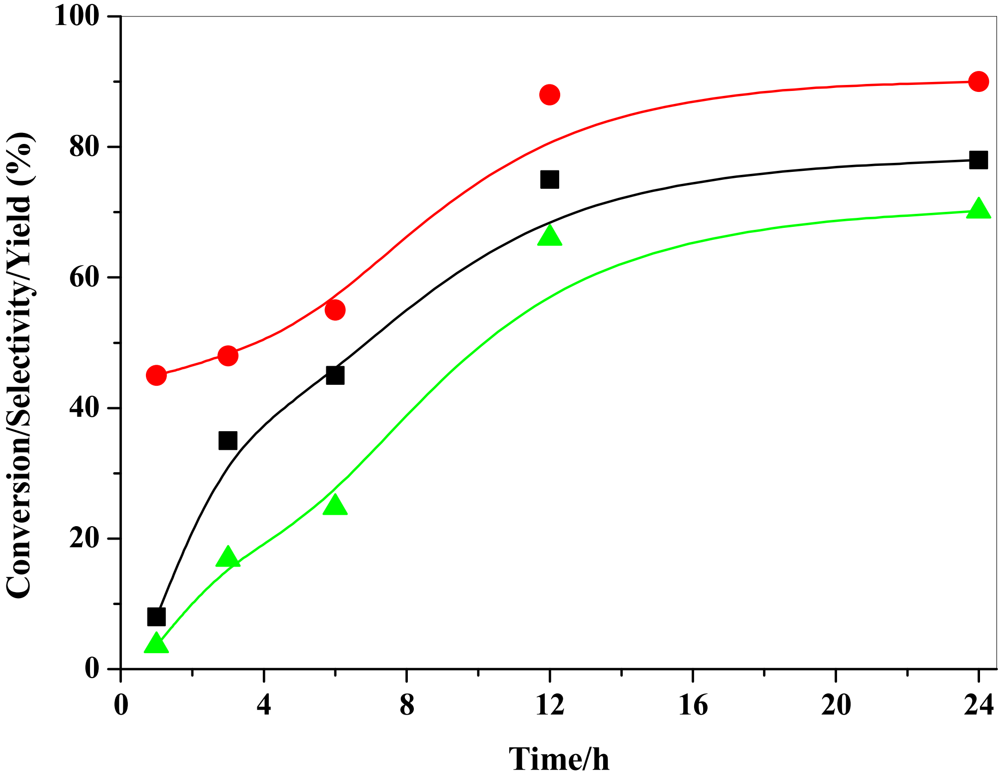

Fig. 12 Effect of time on cyclohexane oxidation.
[■] Conversion of toluene; [●] Selectivity to AA; [▲] Yield of AA;
Reaction Condition: cyclohexane =1g; catalyst = 0.15g; cyclohexane: H_2O_2 molar ratio =1:3; temperature = 70 °C.

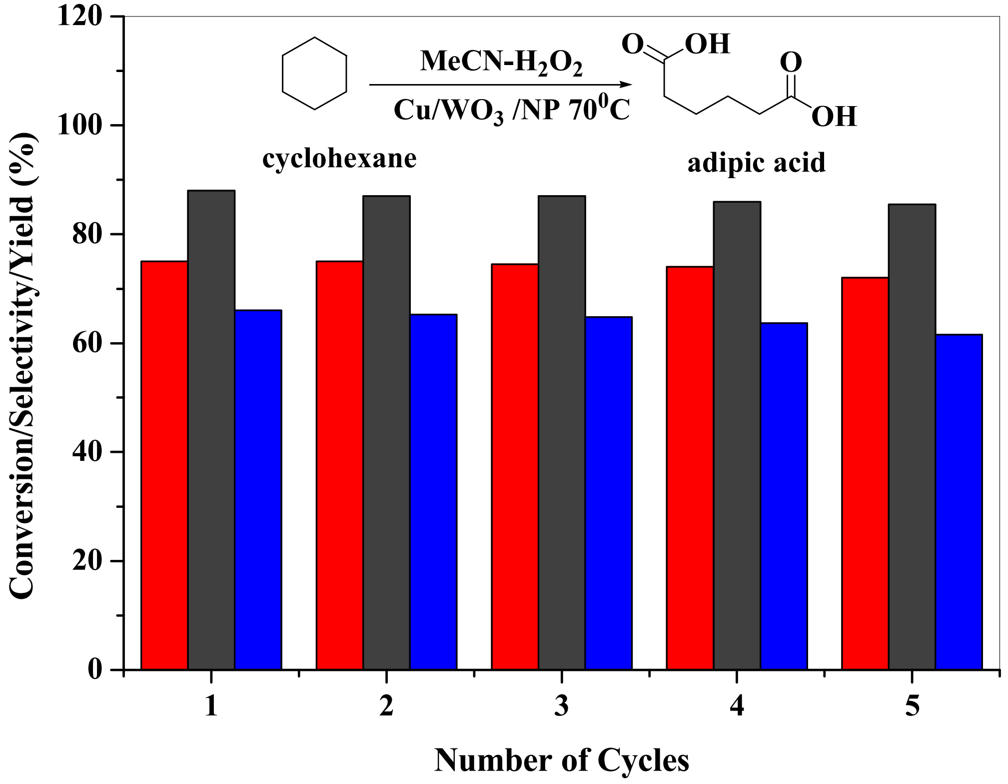

Fig. 13 Recyclability tests of Cu/WO_3 nanoparticles catalyst for the oxidation reaction of cyclohexane to AA.
[🟥] Conversion of cyclohexane; [⬛] Selectivity to AA; [🟦] Yield of AA.

Table 1. Catalytic oxidation of cyclohexane to AA with H_2O_2 as oxidant[a]

Entry	Catalyst	C_C (%)[b]	S_P (%)[c]				Y_{AA}[d] (%)	TON[e]
			AA	Cy-ol	Cy-one	Others		
1	No catalyst	Poor	-	-	>99	-	-	-
2	CuO^{COM}	0.5	-	25	65	10	-	-
3	WO_3^{COM}	1.5	-	10	82	8	-	-
4	$CuO\text{-}WO_3^{IMP}$	2.5	5	8	75	12	0.1	-
5[f]	$Cu(II)/WO_3^{NP2.8}$	75	88	-	6	6	66	119
6[g]	$Cu(II)/WO_3^{NP2.8}$	72	85.5	-	8	6.5	61.5	111
7[h]	$Cu(II)/WO_3^{NP5.5}$	84	55	5	28	12	46.2	46
8[i]	$CuCr_2O_4$ spinel NP	87	-	17	78	5	-	-
9[j]	Ag/WO_3 nano rods	22	-	27	67	6	-	-

[a] Typical reaction conditions: solvent (MeCN) = 10ml, substrate (cyclohexane) = 1g, catalyst= 0.15g, cyclohexane: H_2O_2 (molar ratio) = 1:3, reaction temperature = 70 °C; time = 12 h; [b] C_C = Conversion of cyclohexane based upon the FID-GC using anisole as external standard = [moles of cyclohexane reacted/initial moles of cyclohexane used] x 100; [c] S_P = selectivity to AA = [moles of products produced/ moles of cyclohexane reacted] x 100; [d] Y_{AA} = Yield of AA = $C_C \times S_{AA}/100$; [e] TON = turnover number calculated by moles of AA formed/one mol of Cu in the catalyst present as supported Cu (II) on WO_3; [f] fresh and [g] spent (after 4 recycles) Cu/WO_3 nanoparticles catalyst (loading of Cu is 2.8 %); [h] Cu/WO_3 catalyst (loading of Cu is 5.5 %); [i] catalyst produced following reference 21 and [j] catalyst produced

following reference 16; COM: commercial; IMP: catalyst prepared in impregnation method; NP: nanoparticles.

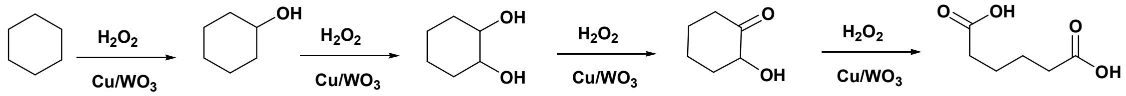

Ref. M.Damm, B.Gutmann and C. O. Kappe, *ChemSusChem,* 2013, **6**, 978.

Scheme 1. Mechanistic path of AA production from cyclohexane over Cu/WO_3 catalyst.

Nanoclusters of Cu (II) Supported on Nanocrystalline W (VI) Oxide: A Potential Catalyst for Single-Step Conversion of Cyclohexane to Adipic Acid

Shankha S. Acharyya,[a] Shilpi Ghosh,[a] and Rajaram Bal[a],*

[a]Catalytic Conversion & Processes Division, CSIR-Indian Institute of Petroleum, Dehradun 248005, India

Corresponding author. Tel.: +91 135 2525917; Fax: +91 135 2660202

E-mail addresses: raja@iip.res.in